

Short Communication

Effect of Sulfurization Temperature on the Preparation of $\text{Cu}_2\text{ZnSnS}_4$ Thin Films for Solar Cells via a Nanoink Coating Method

Qian Li^{1,*}, Yu Hao¹, Yaru Cui^{1,*}, Juan Wang¹, Jinjing Du¹, Miao Wang¹, Jinpeng Hu¹, Tong Shen¹, Lizhen Duan¹, Simin Wang¹, Ke Sun¹, Shan Gao²

¹ School of Metallurgical Engineering, Xi'an University of Architecture and Technology, Xi'an, Shaanxi 710055, China

² AM Incorporation for Metrology and Testing Technology Services, Xi'an, Shaanxi 710055, China

*E-mail: lq@xauat.edu.cn, yaroo@126.com

Received: 3 December 2020 / Accepted: 9 February 2021 / Published: 31 March 2021

High-temperature sulfurization is an effective method for preparing $\text{Cu}_2\text{ZnSnS}_4$ thin-film solar cells with reduced volume resistivity and defect density and a high energy conversion efficiency.

In this paper, a metal oxide precursor (CZTO) prepared by nanoink coating was sulfurized at different temperatures to study the change in the morphology and optimized phase of $\text{Cu}_2\text{ZnSnS}_4$ (CZTS) thin films. XRD-ray diffraction, Raman spectroscopy, SEM and absorption spectra confirmed that the CZTS film annealed at 580°C and had high crystallinity and a uniform particle size, and the absorption coefficient was greater than $10^4/\text{cm}$. Furthermore, a solar cell was fabricated to measure the conversion efficiency of a photoelectric device with the structure Mo/CZTS/CdS/i-ZnO/ITO/Ag. Finally, the $\text{Cu}_2\text{ZnSnS}_4$ solar cell possessed a band gap of 1.48 eV and exhibited a conversion efficiency of 2.08%, with an open-circuit voltage (V_{oc}) of 583 mV, a short-circuit density (J_{sc}) of 7.32 mA/cm^2 and a fill factor (FF) of 48.86%.

Keywords: sulfurization temperature, $\text{Cu}_2\text{ZnSnS}_4$ thin film, crystallinity, conversion efficiency, solar cell

1. INTRODUCTION

CIGS solar cells show a high photoelectric conversion efficiency of 23.3% [1]; however, the use of rare elements (In and Ga) and toxic elements (Cd) limits further development [2,3]. In recent years, with constant research and discovery, the P-type semiconductor $\text{Cu}_2\text{ZnSnS}_4$ (CZTS) has been found to be a potential thin film due to its suitable energy band gap (1.0-1.5 eV), high absorption coefficient ($10^4/\text{cm}$) and more stable perovskite structure than other materials [4-8]. From the points of view of

resource savings and environmental protection, CZTS thin films with nontoxic elements, abundant reserves and easy preparation are desirable substitutes.

According to previous reports, the theoretical efficiency limit of CZTS is 32.2% [9], but the highest actual efficiency of CZTS thin film solar cells prepared by experiments is 12.6% [10], indicating the tremendous upgrade space of CZTS thin-film solar cells. For CZTS thin films, the content and composition of metal elements are important factors directly affecting the efficiency of CZTS thin-film solar cells, so the optimization of the material composition is important for improving the efficiency of photoelectric devices [11]. To date, CZTS thin films can be prepared by evaporation [12,13], sputtering [14,15], electrodeposition [16,17], sol-gel [18,19] and nanoink coating methods, including spinning [20,21] and injection [22,23]. The main advantage of the nanoink coating method is that the resulting materials exhibit ideal properties for requirements, such as a high utilization rate of raw materials and simple equipment. Therefore, the preparation cost of the whole process can be reduced, which is expected to be an industrialized scheme.

It is crucial for CZTS thin films to attain dense surfaces and large particles because decreasing the large volume resistivity and defect density can prevent the formation of secondary phases and promote the growth of thin films, avoiding the appearance of lower short-circuit currents and open-circuit voltages and finally obtaining excellent efficiency for CZTS solar cell devices [24]. Many studies have shown that high-temperature annealing is an effective method for the synthesis of CZTS thin-film solar cells with excellent properties [25,26]. Tang [27] found that sulfurization at low temperature was not conducive to the crystallization of CZTS and was accompanied by the formation of the Cu_xS secondary phase. By comparing the phase and elemental composition of the CZTS thin film at different temperatures, the optimized efficiency of the CZTS solar cell was obtained at 1.22%. Prabeesh [28] prepared pure-phase CZTS through high-temperature sulfurization, proving that the increased crystallinity and band gap were accompanied by temperature. XRD and Raman curves both confirmed the dense and homogeneous microstructure at 500 °C. However, as the temperature increased further, the band gap began to decrease. He [29] investigated the effect of the postannealing process in a H_2S atmosphere on the composition of CZTS thin films. Postannealing enhanced the quality of sulfur in all CZTS thin films, which is beneficial for reducing the amount of sulfur vacancies. Based on the above analysis, it is necessary to further study the effect of sulfurization temperature on the properties of CZTS thin films in the case of large volume resistivity and defect density and finally obtain thin film solar cells with a high-energy conversion efficiency. In this paper, CZTO precursor thin films were prepared by a nanoink coating. Subsequently, the influence of different sulfurization temperatures on the composition, morphology and structure of CZTS thin films was studied, and the application of CZTS thin films on solar energy devices was reported.

2. EXPERIMENT

2.1. Fabrication of $\text{Cu}_2\text{ZnSnS}_4$ thin films

All chemicals used in this paper were analytical grade reagents. The nanoink coating process used to fabricate the $\text{Cu}_2\text{ZnSnS}_4$ thin film is shown in Fig. 1. First, a mixed solution (named S1) of 0.2

mol/L copper sulfate, 0.1 mol/L zinc sulfate and 0.1 mol/L stannous sulfate, as the raw materials, was dissolved in a separator funnel by the parallel flow precipitation method, and a 0.4 mol/L sodium hydroxide solution (named S2) was prepared in another funnel, with 100 ml of deionized water and PVP in the bottom liquid solution (named S3). Subsequently, S1 and S2 were slowly dropped with control into S3 with a pH of 9.5 at 40 °C. To obtain a better mixture, the reaction solution was stirred for 2 h until it was completely homogenized and then filtered to acquire mixed hydroxides. After drying, it was then calcined at 550 °C to obtain a metal oxide. Second, the metal oxide was added to 30 ml of ethanol with methylcellulose and PVP and then ball milled for 6 h at 600 r/min to formulate a nanoink slurry with suitable viscosity. To avoid possible cracks, Mo-sputtered substrates were pre-dried at 40 °C; subsequently, the nanoink was spin-coated on Mo-sputtered substrates at 270 °C to form a metal oxide precursor (CZTO). Subsequently, the CZTO precursor was sulfurized in the annealing process at different temperatures, and finally, a CZTS thin film was obtained. In the following experiments, a $\text{Cu}_2\text{ZnSnS}_4$ solar cell with the structure Mo/CZTS/CdS/i-ZnO/ITO/Ag was considered in this research. In detail, 10 ml of a thiourea solution, 10 ml of CdSO_4 and 14.5 ml of ammonia were first added to 160 ml of DI water and heated at 80 °C for 10 min to deposit CdS on the surface of the CZTS thin film. ZnO and ITO films were deposited on CdS by the RF and DC methods, respectively. Then, Ag glues were used as conductive electrodes, and the total area of the devices was approximately 0.09 cm^2 .



Figure 1. Fabrication of $\text{Cu}_2\text{ZnSnS}_4$ thin films with a nanoink coating process

2.2. Material Characterization

The phase information of the samples was obtained from XRD ($\lambda=1.54 \text{ \AA}$, 40 kV acceleration voltage). The compositions of the films were determined by EDX (Oxford X-Max20). The surface and cross-sectional morphologies of the film were investigated with FESEM (TESCAN MIRA3 LMU). Further phase differentiation was tested by Raman spectroscopy (LABRAM-HR). XPS studies were carried out with Mg $K\alpha$ radiation (1253.6 eV) on an ESCA MULTIPLEX-1600 spectrometer. The transmittance spectrum of the CZTS film was obtained by a UV-Vis spectrophotometer (HITACHI U-4100) with a wavelength range of 300-900 nm. The formula relating band gap (E_g) to photon energy ($h\nu$) was expressed as $\alpha h\nu = A(h\nu - E_g)^n$, where α is the absorption coefficient. The current-voltage (J-V) characteristics of the CZTS solar cell were measured on an Oriel mode 94023A measurement system.

3. RESULTS AND DISCUSSION

3.1. Preparation of the metal oxide precursor thin film

The nanoink coating process was one of the methods used for the fabrication of $\text{Cu}_2\text{ZnSnS}_4$ thin films [30,31]. Hydroxides were fabricated by parallel flow precipitation and then calcined to produce a metal oxide. The nanoink was formed by dispersing the metal oxide in ethanol with PVP and methylcellulose. Subsequently, the metal oxide precursor was obtained by spin-coating on Mo-sputtered glass substrates.

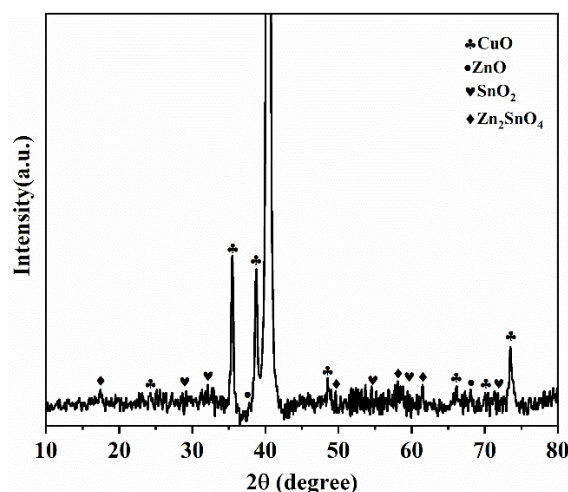


Figure 2. XRD patterns of the metal oxide precursor

XRD patterns of the metal oxide precursor (Fig. 2) showed several strong peaks attributed to metal oxide mixtures, namely, CuO, ZnO and SnO₂. In addition to these strong metal oxide peaks, peaks attributed to the Zn₂SnO₄ phase can also be found due to the reaction of ZnO and SnO₂ during high-temperature annealing [28,32]. For the preparation of the CZTS thin film, ZnO in the component not only inhibited the formation of MoS₂ but also acted as the source of Zn in CZTS. In addition, the high stability of SnO₂ in the CZTO precursor greatly prevents the loss of Sn at high sulfurization temperatures [33], so the introduction of oxygen atoms in the precursor can improve the growth of CZTS.

3.2. Effect of sulfurization temperature on the $\text{Cu}_2\text{ZnSnS}_4$ thin film

The chemical compositions of $\text{Cu}_2\text{ZnSnS}_4$ thin films annealed at different temperatures from 250 to 580 °C are listed in Fig. 3. The mole ratio of Cu/(Zn+Sn) remained almost unchanged with increasing temperature. From 250 to 500 °C, the mole ratio of Zn/Sn dramatically increased and then decreased. Finally, it was noticed that the mole ratio of Zn/Sn increased slightly at 580 °C. The reason for this may be that Sn and S reacted to produce unstable SnS₂, which readily reverted to SnS, resulting in the loss of Sn. However, with increasing temperature, the S powder was completely gasified, increasing vapor

pressure, so SnS and S later transformed into SnS₂, which was absorbed into the thin film. Finally, the mole ratio of Zn/Sn decreased [34]. Above 250 °C, the mole ratio of S/metal were more than 1, indicating that the S atom was fully incorporated into the thin film. The reaction $2\text{CuO} + 3\text{S} = 2\text{CuS} + \text{SO}_2$ could be carried out.

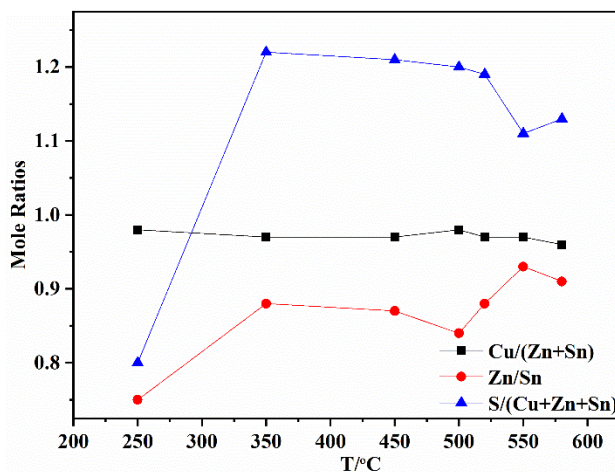


Figure 3. Chemical mole ratio of Cu₂ZnSnS₄ thin films annealed at different temperatures from 250 to 580 °C

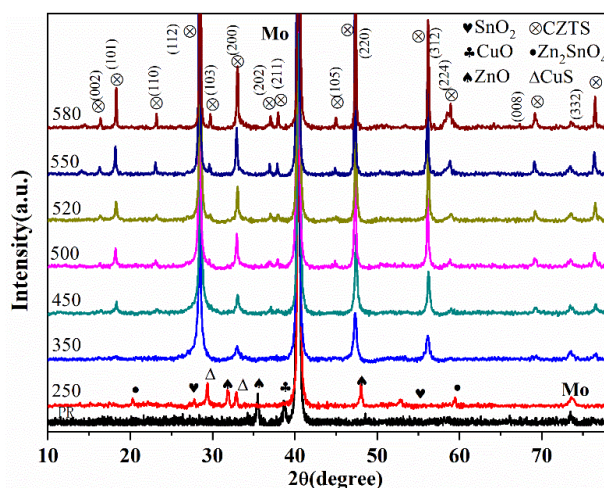


Figure 4. XRD patterns of the precursor (PR) and Cu₂ZnSnS₄ thin film annealed from 250 to 580 °C

XRD patterns of the precursor (PR) and Cu₂ZnSnS₄ thin film annealed from 250 to 580 °C are presented in Fig. 4. The main diffraction peaks of CuO totally disappeared, which suggested that CuO first converted into CuS at 250 °C; in contrast, the other metal oxides were stable. The Cu₂ZnSnS₄ phase was first observed at 350 °C, and the peaks at $2\theta=28.5^\circ$, 47.3° and 56.1° became increasingly apparent and sharper, corresponding to the (112), (220), and (312) planes [35], which are the preferential orientations of the Cu₂ZnSnS₄ thin film (JCPDS no. 26-0575). When the annealing temperature reached 450 °C, the CuS and Zn₂SnO₄ phases disappeared, and the (202), (224) and (008) peaks of the Cu₂ZnSnS₄

thin films became sharper. The full width at half maximum (FWHM) of the main characteristic peaks of $\text{Cu}_2\text{ZnSnS}_4$ decreased, indicating that the crystalline property was gradually optimized. In particular, at 580 °C, no other obvious peaks, such as SnS or SnS_2 peaks, were found. The three main peaks corresponding to the (112), (220) and (312) crystal planes demonstrated that the $\text{Cu}_2\text{ZnSnS}_4$ thin film grew with a preferred grain orientation at 580 °C because increasing the temperature was unfavourable to the stability of the CZTS thin film; otherwise, a secondary phase, such as SnS_x , appeared [25].

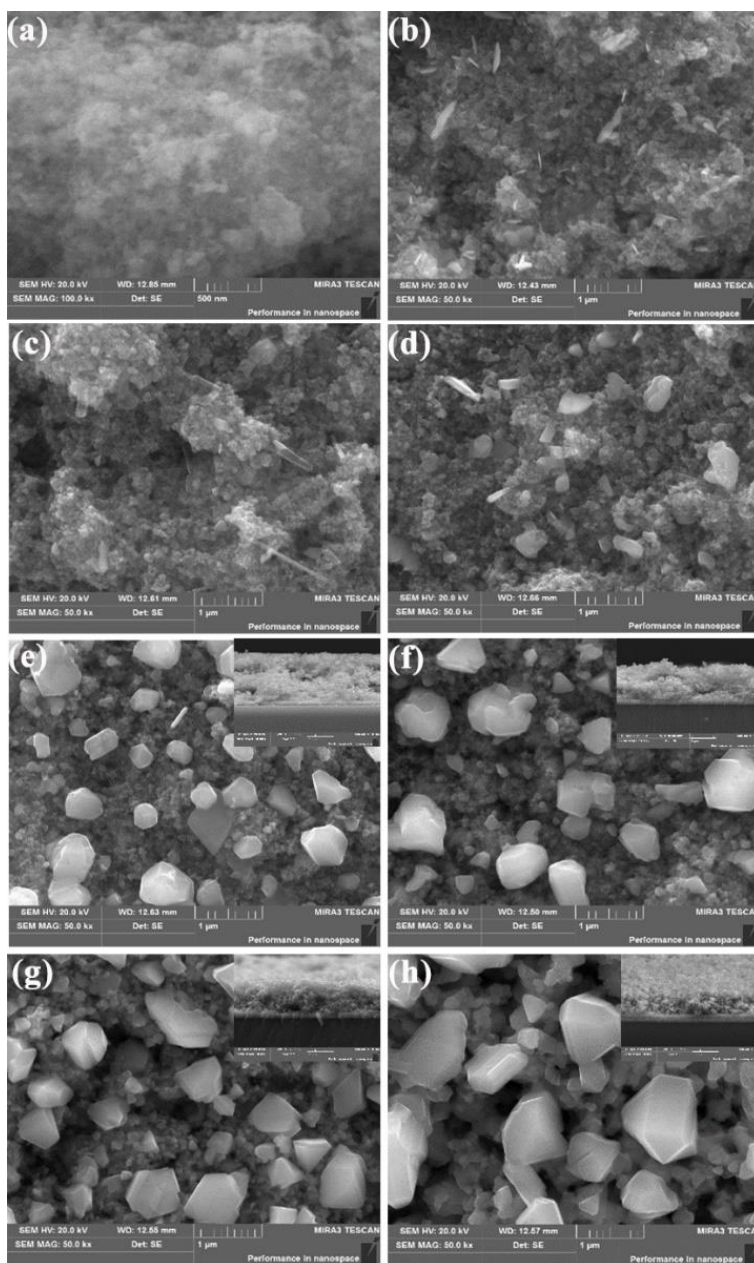


Figure 5. SEM image of the metal oxide precursor (CZTO) (a) and $\text{Cu}_2\text{ZnSnS}_4$ thin films annealed at (b) 250 °C; (c) 350 °C; (e) 450 °C; (e) 500 °C; (f) 520 °C; (g) 550 °C; and (h) 580 °C (the inset shows the cross-sectional morphology from 500 to 580 °C)

The surface SEM images of thin films sulfurized at different temperatures are illustrated in Fig. 5. There were no obvious large particles on the surface of the thin film at 250 °C, and some white stripes were distributed on it, presumably due to Cu_xS particles. After annealing at 350 °C, the stripes of the particles became larger. Then, the particles appeared on the surface of the annealed thin film accompanied by a small amount of flocs at 450 °C, which may be the unreacted remainder of Cu_xS at the bottom of the thin film. No obvious flocs were observed on the surface of the thin film at 500 °C, and the crystalline grains became larger with increasing sulfurization temperature. The surface of the particles grew obviously, with a size of approximately 200-400 nm at 520 °C, showing that the crystallinity was greatly improved. After annealing at 550 °C, the size of the larger particles was approximately 500 nm. Up to 580 °C, the $\text{Cu}_2\text{ZnSnS}_4$ thin film showed a compact and uniform morphology, with a particle size of approximately 1 μm . In contrast to the results obtained at temperatures from 500 to 550 °C, the cross-sectional view of the growing region lacked burrs and was smoother, indicating that the crystalline quality of the thin film was further improved and that the thin film basically covered $\text{Cu}_2\text{ZnSnS}_4$.

However, $\text{Cu}_2\text{ZnSnS}_4$, Cu_2SnS_3 and ZnS have very similar XRD diffraction patterns. Therefore, XRD analysis is not accurate for identifying $\text{Cu}_2\text{ZnSnS}_4$ [36,37]. Hence, Raman spectroscopy was used to improve phase differentiation. The main peaks are located at 167, 287, 334-338, 354 and 372 cm^{-1} for $\text{Cu}_2\text{ZnSnS}_4$, 351 cm^{-1} for Cu_2SnS_3 , 350 cm^{-1} for ZnS and 475 cm^{-1} for Cu_2S [38-41].

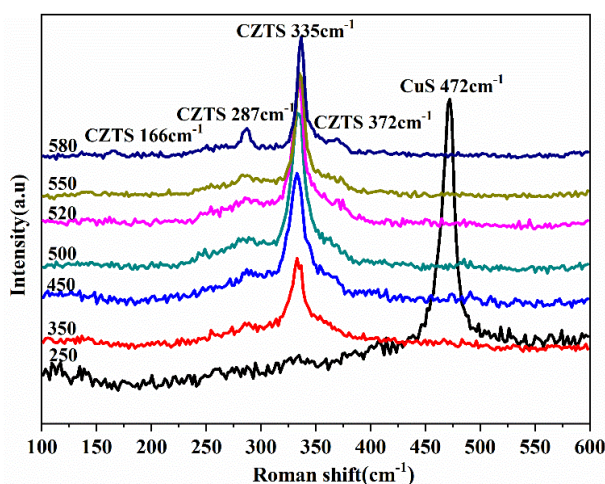


Figure 6. Raman analysis of the metal oxide precursor (CZTO) and $\text{Cu}_2\text{ZnSnS}_4$ thin film annealed at 250, 350, 450, 500, 520, 550 and 580 °C

The Raman analysis of the $\text{Cu}_2\text{ZnSnS}_4$ thin film annealed at different temperatures is shown in Fig. 6. The CuS phase was detected in the metal oxide precursor (CZTO) with a strong peak at 472 cm^{-1} at 250 °C. The appearance of the CuS phase at low temperature confirmed the XRD analysis results. The peak at 472 cm^{-1} related to CuS obviously disappeared at 350 °C; additionally, the peak at 335 cm^{-1} corresponding to the main phase of $\text{Cu}_2\text{ZnSnS}_4$ was also detected. As the annealing temperature increased, the peak of CuS disappeared, and the peaks at 287 cm^{-1} and 335 cm^{-1} related to $\text{Cu}_2\text{ZnSnS}_4$ became increasingly obvious. At the same time, the location of the peak with the highest intensity shifted

to the low frequency region, which is attributable to the gradual diffusion of Zn atoms into the CTS lattice, causing a redshift of CTS to the $\text{Cu}_2\text{ZnSnS}_4$ peak. Finally, CTS gradually changed into $\text{Cu}_2\text{ZnSnS}_4$. This result corresponded to the results obtained from both the XRD and FESEM analyses. Sharp peaks could be observed at 166 cm^{-1} , 287 cm^{-1} and 335 cm^{-1} at $580\text{ }^\circ\text{C}$. Simultaneously, secondary phase SnS_2 and SnS were not detected [32].

XPS analysis of the $\text{Cu}_2\text{ZnSnS}_4$ thin film annealed at $580\text{ }^\circ\text{C}$ is shown in Fig. 7. The peaks of Cu $2p_{3/2}$ and Cu $2p_{1/2}$ (a) at 934.5 eV and 954.2 eV with a difference in energy of 19.7 eV proved the formation of Cu(I) [41,42]. The peak separation of 23.1 eV was accompanied by Zn(IV) $2p_{3/2}$ and $2p_{1/2}$ core levels in Fig. 7(b), indicating the presence of Zn^{+} [42]. The presence of two peaks at 486.5 and 495 eV with a peak energy difference of 8.5 eV suggests the presence of Sn(IV) [42,43]. With a peak splitting of 1.2 eV , S(II) (d) existed in the formation of $\text{Cu}_2\text{ZnSnS}_4$ [35]. The elements Cu, Zn, Sn and S changed in the annealing process during the phase evolution of the $\text{Cu}_2\text{ZnSnS}_4$ thin film. The binding energy values agreed with previously reported values [45], which were confirmed with XRD and Raman analysis.

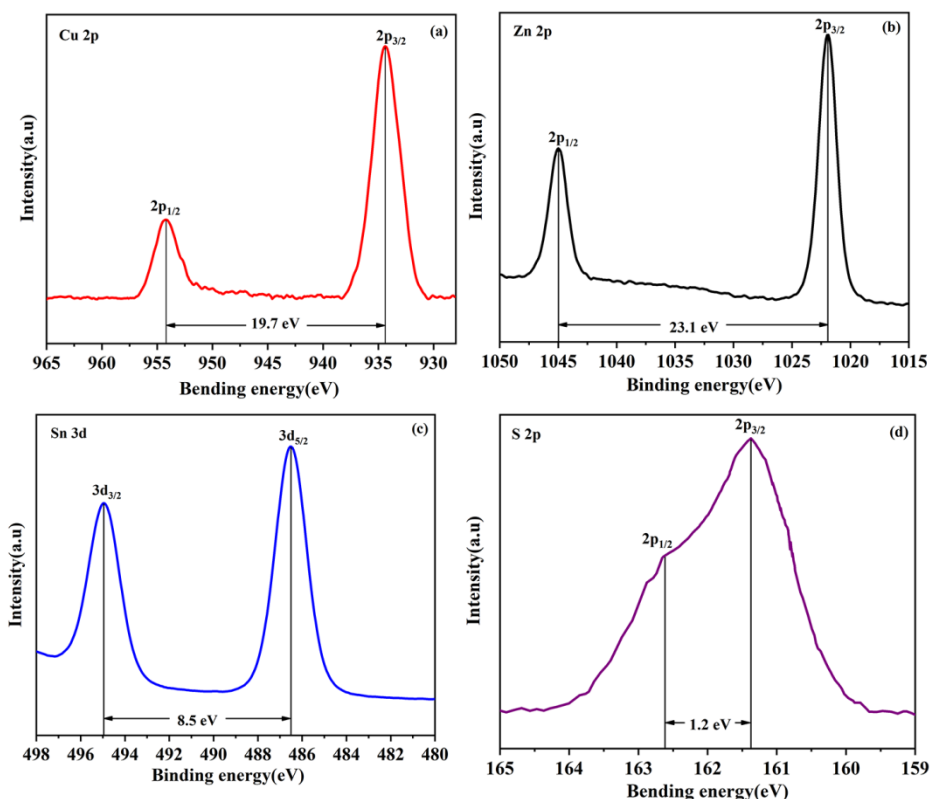


Figure 7. XPS spectra of the $\text{Cu}_2\text{ZnSnS}_4$ thin film sulfurized at $580\text{ }^\circ\text{C}$

The absorption coefficient (a) and $(\alpha h\nu)^2$ vs $h\nu$ plot of $\text{Cu}_2\text{ZnSnS}_4$ absorber layers (b) at different temperatures are displayed in Fig. 8. By setting $\alpha=0$, the optical band gap of the sample can be obtained by extrapolating the linear part of the $(\alpha h\nu)^2$ pairs of $h\nu$ curves [43]. The band gap values calculated based on this method at different sulfurization temperatures ranged from 1.2 to 1.5 eV , which is

consistent with the reported values [36,46]. The band gap was not obviously affected from 500 °C to 580 °C.

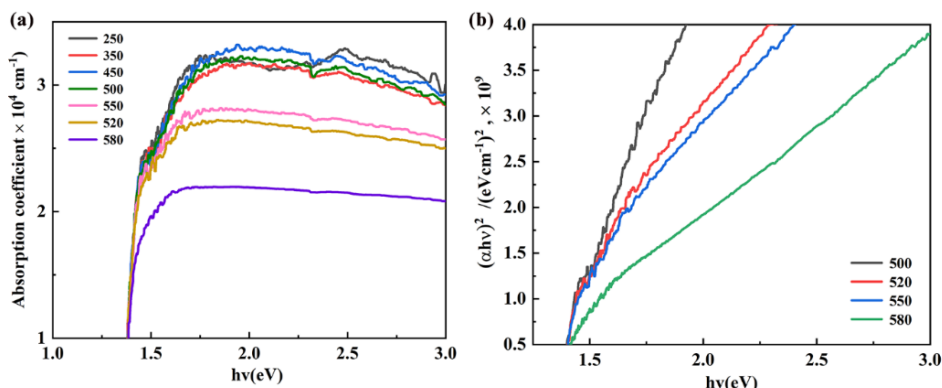


Figure 8. (a) Absorption spectra of Cu₂ZnSnS₄ thin films annealed from 250 to 580 °C. (b) $(\alpha hv)^2$ versus photon energy (hv) plot of Cu₂ZnSnS₄ thin films fabricated at 500, 520, 550 and 580 °C

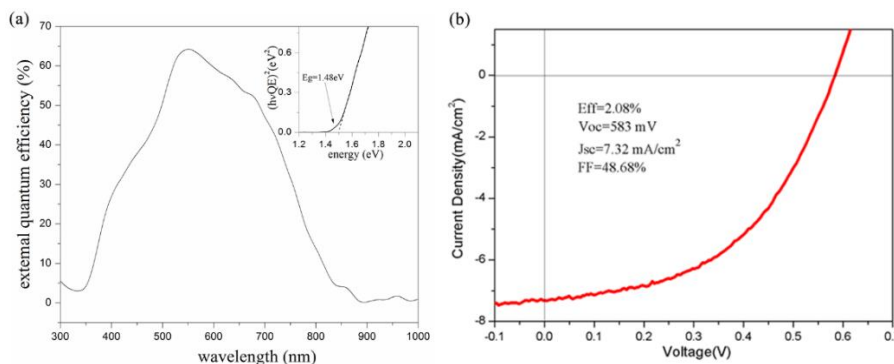


Figure 9. (a) EQE curve of the CZTS solar cell annealed at 580 °C (the inset shows the band gap (E_g) of CZTS obtained by linear fitting with the EQE curve). (b) J-V curve of the Cu₂ZnSnS₄ solar cell

Table 1. Parameters of Cu₂ZnSnS₄ thin-film devices, as well as those of some published pure sulfide devices

Sample	Voc (mV)	Jsc (mA cm ⁻²)	FF (%)	Efficiency (%)	Eg (eV)
CZTS device[18]	370	13.52	45	2.25	1.42
CZTS device[27]	320	9.28	41	1.22	1.35
CZTS device[28]	380	17.19	46	3.02	1.45
CZTS device[32]	505	10.5	30.3	1.6	1.48
This work	583	9.28	48.86	2.08	1.48

Fig. 9(a) shows the EQE curve of the CZTS solar cell annealed at 580 °C. The curve shows that the EQE was highest at a wavelength of 550 nm and was close to 65%. When the wavelength was lower

than 550 nm, the EQE value decreased with increasing wavelength, which was attributed to the decreased absorption of the window layer and CdS buffer layer. Then, the EQE value continued to decline with increasing wavelength due to the decreased photon absorption of the CZTS optical absorber [47]. The inset of Fig. 9(a) shows the band gap (E_g) of CZTS obtained by linear fitting with the EQE curve, and the calculated band gap was 1.48 eV, which is in agreement with the theoretical band gap of the CZTS solar cell [48]. The current density-voltage (J-V) curve of the CZTS solar cell with the structure Mo/CZTS/CdS/i-ZnO/ITO/Ag is displayed in Fig. 9(b), and the device parameters are shown in Table 1. The current density is reduced, which may be due to the short-circuit current loss caused by the larger series resistance, while the impurity phase Cu_2SnS_3 with a narrow band gap will lead to a decrease in the open circuit voltage [32]. The conversion efficiency was 2.08%, with an open-circuit voltage (V_{oc}) of 583 mV, a short-circuit current density (J_{sc}) of 7.32 mA/cm^2 and a fill factor (FF) of 48.68%. The above results showed that the CZTS thin film prepared by high-temperature sulfurization was well situated for the good performance of the photoelectric device.

4. CONCLUSION

In this study, a high-temperature sulfurization approach was employed for the synthesis of $\text{Cu}_2\text{ZnSnS}_4$ (CZTS) thin-film solar cells by the postannealing of the CZTO precursor. The results showed that high-temperature sulfurization could reduce the large volume resistivity and defect density and result in a high short-circuit density and a high open-circuit voltage. The XRD pattern demonstrated that more oxides were present in the CZTS thin film sulfurized at 250 °C, which was caused by the incomplete sulfuration of the CZTO precursor. The phases of CZTS appeared at the 350 °C sulfurization temperature, suggesting a change from CZTO to CZTS. At 580 °C, the highest-crystallinity product appeared at 580 °C, and no obvious secondary phase was observed. The Raman spectrum further confirms this conclusion. Additionally, a CZTS thin film with a dense and uniform surface with large particles was obtained by annealing at 580 °C. The further synthesized CZTS solar cell exhibited a band gap of 1.48 eV, which was close to the theoretical band gap value of 1.5 eV. The optical properties of the CZTS solar cell were tested by obtaining a J-V curve, exhibiting a conversion efficiency of 2.08%, an open-circuit voltage (V_{oc}) of 583 mV, a short-circuit density (J_{sc}) of 7.32 mA/cm^2 and a fill factor (FF) of 48.86%.

ACKNOWLEDGEMENTS

This work was supported by the National Natural Science Foundation of China (No. 51504181 and No. 51674186), Natural Science Foundation of Shaanxi Province (No. 2020JQ-679 and No. 2019JQ-761), Shanxi Key Laboratory Project (No. 20JS064), Key Laboratory Project of Xi'an (No. 2019219914SYS014CG036), Innovation and Entrepreneurship Training Program of Xi'an University of Architecture and Technology in 2020 (No. S202010703126), and 15th batch of Undergraduate Scientific Research and Training Program of Xi'an University of Architecture and Technology in 2020: Controllable preparation of SnS/GO thin film electrode materials, Electrochemical performance of SnS/GO thin film electrode materials.

References

1. M.A. Green, K. Emery, Y. Hishikawa, W. Warta and E.D. Dunlop, *ProgPhotovoltaics.*, 24 (2016) 905.
2. K. Rawat and P.K. Shishodia, *Superlattice. Microst.*, 122 (2018) 444.
3. Q. Wen, Y. Li, J. Yan, J. Wang and C. Wang, *Superlattice. Microst.*, 85 (2015) 331.
4. S Susanne and S Susan, *ProgPhotovoltaics.*, 20 (2012) 512.
5. A. Tumbul, F. Aslan, A. Goktas and I.H. Mutlu, *J. Alloy Compd.*, 781 (2019) 280.
6. T. Ahmet, A. Ferhat, G. Abdullah, Z.Z. Maharram and K. Ahmet, *Mater. Chem. Phys.*, 258 (2021) 123997.
7. N. Azmi, P. Chelvanathan, Y. Yusoff, M.T. Ferdaous, A. W. M. Zuhdi, S. K. Tiong, and N. Amin, *Mater. Lett.*, 285 (2021) 129177.
8. K. Kaur, Nisika, A.H. Chowdhury, Q. Qiao and M. Kumar, *J. Alloy Compd.*, 854 (2021) 157160.
9. Q. Guo, H. W. Hillhouse and R. Agrawal, *J. Am. Chem. Soc.*, 131 (2009) 11672.
10. M.A. Green, E.D. Dunlop, D.H. Levi, J. Hohl-Ebinger, M. Yoshita and A.W.Y. Ho-Baillie, *ProgPhotovoltaics.*, 28 (2020) 3.
11. W.S. Liu, S.Y. Chen, C.S. Huang, M.Y. Lee and H.C. Kuo, *J. Alloy Compd.*, 853 (2021) 157237.
12. C. Sripan, V.E. Madhavan, A.K. Viswanath and R. Ganesan, *Mater. Lett.*, 189 (2017) 110.
13. N.J. Choudhari, Y. Raviprakash, F. Bellarmine, M.S.R. Rao and R. Pinto, *Sol. energy.*, 201 (2020) 348.
14. C. Ma, X. Lu, B. Xu, F. Zhao, X. An, B. Li, F. Yue, J. Jiang, Y. Chen, L. Sun and J. Chu, *J. Alloy Compd.*, 853 (2020) 153329.
15. S. Pandahrkar, A. Punde, M. Nasane, V. Doiphode, P. Shinde, P. Vairale, Y. Hase, A. Bhorde, A. Waghmare, S. Rondiya, M. Prasad and S. Jadkar, *Mater. Today.*, (2020).
16. Y. H. Khattak, F. Baig, H. Toura, I. Harabi, S. Beg and B.M. Soucase, *Appl. Surf. Sci.*, 497 (2019).
17. H. Toura, Y.H. Khattak, F. Baig, B.M. Soucase, M.E. Touhami and B. Hartiti, *Curr. Appl. Phys.*, 19 (2019) 606.
18. L. Dong, S. Cheng, Y. Lai, H. Zhang and H. Jia, *Thin Solid Film.*, 626 (2017) 168.
19. A. Ashfaq, J. Hacob, N. Bano, M. Ajza-Un-Nabo, W. Ahmad, A. Ali, W. Anmad, K. Mahmood, M.I. Arshad, S. Ikram, U. Rehman, N. Amin and S. Hussain, *Ceram. Int.*, 45 (2019) 10876.
20. A. Kumar, P. Ranjan, A. Thakur, *Mater. Today.*, 5 (2018) 99.
21. B. Liu, J. Guo, R. Hao, L. Wang, K. Gu, S. Sun and A. Aierken, *Sol. Energy.*, 201 (2020) 219.
22. Y. Altowairqi, A. Alsubaie, K.P. Stroh, I.G. Perez-Marin, L. Bowen, M. Szablewski and D.P. Halliday, *Mater. Today.*, 18 (2019) 473.
23. G. Agarwal, and B. Tripathi, *Mater. Today.*, (2021).
24. S. Exarhos, E. Palmes and L. Mangolini, *Thin Solid Film.*, 684 (2019) 21.
25. J.J. Scragg, T. Ericson, T. Kubart, M. Edoff and C. Platzer-Bjorkman, *Chem. Mater.*, 23 (2011) 4625.
26. Y. Sui, D. Jiang, Y. Wu, W. He, F. Zeng, Z. Wang, F. Wang, B. Yao and L. Yang, *Ceram. Int.*, 47 (2021) 3054.
27. D. Tang, Q. Wang, F. Liu, L. Zhao, Z. Han, K. Sun, Y. Lai, J. Li and Y. Liu, *Surf. Coat. Tech.*, 232 (2013) 53.
28. P. Prabeesh, V.G. Sajeeh, I.P. Selvam, M.S. D. Bharati, G.M. Rao and S.N. Potty, *Sol. Energy.*, 207 (2020) 419.
29. J. He, L. Sun, K.Z. Zhang, W.J. Wang, J.C Jiang, Y. Chen, P.X. Yang, J.H. Chu, and C. J, *Appl. Surf. Sci.*, 264 (2013) 133.
30. C. Li, B. Yao, Y. Li, Z. Xiao, Z. Ding, H. Zhao, L. Zhang and Z. Zhang, *J. Alloy Compd.*, 643 (2015) 152.
31. K. Kapusta, M. Drygas, J. Janik and Z. Olejniczak, *J. Mater Res. Tech.*, 9 (2020) 13320.
32. X. Jin, J. Li, G. Chen, C. Xue, W. Liu and C. Zhu, *Sol. Energ. Mater. Sol. C.*, 146 (2016) 16.

33. G. Chen, C. Yuan, J. Liu, Z. Huang, S. Chen, W. Liu, G. Jiang and C. Zhu, *J. Power. Sources.*, 276 (2015) 45.
34. M.A. Olgar, A. Seyhan, A.O. Sarp and R. Zan, *Superlattice. Microst.*, 146 (2020) 106669.
35. T. Wang, S. Pu, S. Wang, S. Yang, X. Li and X. Li, *Opt. Mater.*, 108 (2020) 110217.
36. P. Prabeesh, P. Saritha, I.P. Selvam and S.N. Potty, *Mater. Res. Bull.*, 86 (2017) 295.
37. A. Singh, H. Geaney, F. Laffir and K. Ryan, *J. Am. Soc.*, 134 (2012) 2910.
38. J. Tao, K. Zhang, C. Zhang, L. Chen, H. Cao, J. Liu, J. Jiang, L. Sun, P. Yang and J. Chu, *Chem. Commun.*, 51 (2015) 10337.
39. J. Scragg, T. Ericson, X. Fontane, V. Izquierdo-Roca, A. Perez-Rodriguez, T. Kubart, M. Edoff and C. Platzer-Bjorkman, *Prog. Photovoltaics.*, 22 (2014) 10.
40. E. Garcia-Llamas, J.M. Merino, R. Gunder, K. Neldener, D. Greiner, A. Steigert, S. Giraldo, V. Izquierdo-Roca, E. Saucedo, M. Leon, S. Schorr and R. Caballero, *Sol. Energy.*, 141 (2017) 236.
41. X. Liu, R. Hao, F. Chang, Y. Li, K. Gu, L. Wang, B. Liu and J. Guo, *Z. Naturforsch. A.*, 72 (2018) 957.
42. C. Khélia, K. Boubaker, T.B. Nasrallah, M. Amlouk, and S. Belgacem, *J. Alloy Compd.*, 477 (2009) 461.
43. M.P. Suryawanshi, S.W. Shin, U.V. Ghorpade, K.V. Gurav, C.W. Hong, P.S. Patil, A.V. Moholkar and J.H. Kim, *J. Alloy Compd.*, 671 (2015) 509.
44. M. Voshwakarma, K. Agrawal, J. Hadermann and B.R. Mehta, *Appl. Surf. Sci.*, 507 (2020) 145043.
45. J. Xu, X. Yang, Q. Yang, T.L. Wong and C.S. Lee, *J. Phys. Chem. C.*, 116 (2012) 19718.
46. A. Wangperawong, J.S. King, S.M. Herron, B.P. Tran, K. Pangan-Okimoto and S.F. Bent, *Thin Solid Film.*, 519 (2011) 2488.
47. S. Zhang, N.D. Pham, T. Tesfamichael, J. Bell and H. Wang, *Sustain. Mater. Techno.*, 18 (2018) e00078.
48. J.J. Scragg, P.J. Dale, and L.M. Peter, *Electrochem. Commun.*, 10 (2008) 639.